RESEARCH ARTICLE

Hydrophobic NIR Photocatalysts for High-Throughput Aqueous RAFT Polymerization: Achieving Ultrahigh Molecular Weights with 4-ppm Dye Colloids

Ruoyu Li,[a] Steven P. Armes,[c] and Zesheng An*[a,b]

[a] Dr. R. Li, Prof. Z. An
State Key Laboratory of Supramolecular Structure and Materials
College of Chemistry, Jilin University
Changchun, China
E-mail: anzesheng@jlu.edu.cn
[b] Prof. Z. An
Key Laboratory for Molecular Enzymology and Engineering of Ministry of Education
School of Life Sciences, Jilin University
Changchun, China
[c] Prof. S. P. Armes
School of Mathematical and Physical Sciences
University of Sheffield
Sheffield, South Yorkshire, S3 7HF, UK

Supporting information for this article is given via a link at the end of the document.

Abstract: Near-infrared (NIR) photocontrolled radical polymerization offers the opportunity to combine NIR's deep-tissue penetration and biocompatibility with the precision and versatility afforded by controlled polymerization. However, its development is hindered by the scarcity of water-soluble NIR photocatalysts. Moreover, only relatively low molecular weights have been achieved to date. To overcome these limitations, we have prepared colloidal NIR photocatalysts to conduct efficient reversible addition-fragmentation chain transfer (RAFT) polymerization in aqueous media. Combined with glucose oxidase for in situ degassing and H_2O_2 generation, such NIR dye particles photosensitize H_2O_2 to produce a controlled flux of hydroxyl radicals. This novel enzyme-NIR strategy enables high-throughput RAFT polymerization of various vinyl monomers with excellent control. Notably, ultrahigh molecular weight (M_n > 1,000 kg mol^{-1}) homopolymers can be obtained for polymerizations conducted through an opaque biological barrier at ultralow photocatalyst loadings (4 ppm). Thus such enzyme-NIR formulations enable precision polymer syntheses even in physiologically relevant environments.

Introduction

Reversible deactivation radical polymerization (RDRP) enables precise control over molecular weight, dispersity (*Đ*), topology, sequence, and end-group functionality, which are essential for tailoring advanced biomaterials, nanomedicines, and functional devices.[1] Photo-mediated RDRP has emerged as a powerful and rapidly evolving subset of these techniques, leveraging light as a clean energy source to achieve spatiotemporal control under mild conditions.[2] However, conventional photo-mediated RDRP predominately employs either UV or short-wavelength visible light. These wavelengths often induce undesirable side reactions, offer limited biocompatibility, and provide poor penetration through biological media.[3]

Near-infrared (NIR) light offers a promising alternative to circumvent these limitations. In particular, its longer wavelength enables significantly deeper penetration through biological tissues while minimizing photo-damage and side reactions due to its lower photon energy.[4] The potential of NIR light has been demonstrated for various applications including biomedical imaging, photothermal therapy, drug release, and environmental sensing.[5] Given its distinctive characteristics, NIR photocontrolled RDRP has attracted significant interest for the preparation of biocompatible polymers, self-healing hydrogels, and polymer nanoparticles in biologically relevant environments such as aqueous solution or beneath biological tissues.[6]

Due to its environmental friendliness and biocompatibility, NIR-mediated aqeuous RDRP has recently attracted great research interest. For example, Qiao et al. reported NIR-mediated reversible addition−fragmentation chain transfer (RAFT) polymerization in water using a self-assembled carboxylated porphyrin as a photocatalyst.[7] Boyer et al. utilized water-soluble tetrasulfonated zinc phthalocyanine for NIR photosensitization of H_2O_2 to initiate RAFT polymerization.[6g, 8] Zhang and Cheng recently synthesized a series of water-soluble zinc phthalocyanine NIR photocatalysts for RAFT polymerization.[9] Matyjaszewski and co-workers established an oxygen-tolerant aqueous atom transfer radical polymerization (ATRP) formulation suitable for either red light or NIR irradiation, employing a dual catalytic system comprising methylene blue and Cu for high-throughput open-air synthesis.[10] Nevertheless, current NIR-mediated aqueous polymerization protocols still suffer from complex photocatalyst synthesis, limited catalyst activity, and restricted access to high molecular weights.[6f, 11] The low NIR photon energy typically results in low polymerization efficiency and requires high photocatalyst loadings (> 20 ppm).[12]

Herein, we report the use of hydrophobic NIR photocatalysts as colloidally stable particles for efficient aqueous RAFT polymerization, yielding a series of well-defined homopolymers with low dispersities over broad molecular weight ranges. Hydrophobic NIR photocatalysts are dispersed in water using a non-ionic surfactant to form stable colloidal particles (Scheme 1a). When combined with glucose oxidase (GOx) for in situ oxygen scavenging and H_2O_2 generation, these photocatalyst particles efficiently photosensitize H_2O_2 to produce a controlled flux of hydroxyl radicals. This enables oxygen-tolerant, high-throughput

RAFT polymerization to be conducted under NIR irradiation in microtiter plates (Scheme 1b). Remarkably, this enzyme-NIR system enables ultrahigh molecular weight (UHMW) to be achieved even when polymerization is conducted through a biological barrier (porcine tissue), demonstrating unprecedented NIR penetration and efficiency.

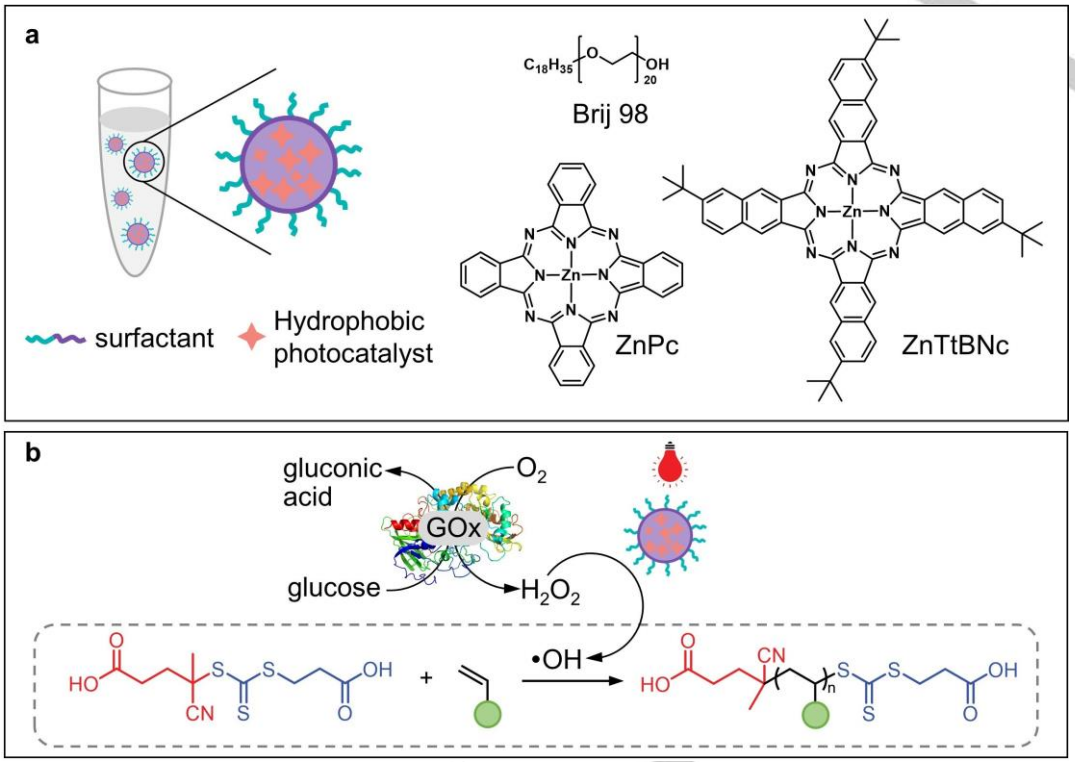

Scheme 1. a) Schematic representation of surfactant-dispersed hydrophobic photocatalysts in water and chemical structures of the non-ionic surfactant (Brij 98) and photocatalysts. b) Schematic representation of enzyme-NIR cascade for RAFT polymerization. Glucose oxidase (GOx) catalysis converts oxygen into H_2O_2, which is in situ photosensitized by NIR photocatalyst particles to produce hydroxyl radicals, thus initiating controlled aqueous RAFT polymerization.

Results and Discussion

Construction of Enzyme-NIR cascade catalysis

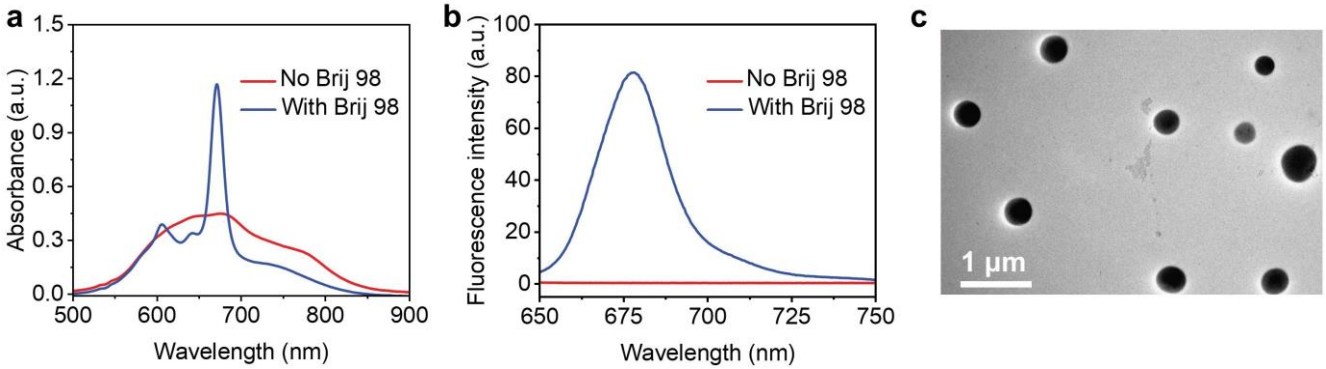

Figure 1. a) Visible absorption and b) fluorescence spectra (excitation wavelength = 635 nm) recorded for ZnPc in the absence or presence of Brij 98 in phosphate buffer (0.2 M, pH 5.7). c) TEM micrograph of Brij 98-stabilized ZnPc particles.

To enable efficient aqueous RAFT polymerization, the hydrophobic NIR photocatalyst was dispersed in water using a suitable surfactant as colloidally stable particles.[13] Initially, zinc phthalocyanine (ZnPc) was selected as a representative hydrophobic photocatalyst for its well-known capacity to photosensitize peroxides and hence generate radical species under NIR light irradiation.[14] A widely used nonionic surfactant, Brij 98, was selected owing to its ready availability and excellent biocompatibility.[15] First, we studied the stabilization effect of Brij 98 on ZnPc. Colloidal particles were prepared by dissolving the hydrophobic photocatalyst and Brij 98 in DMF, followed by addition of this DMF solution to phosphate buffer (0.2 M, pH 5.7),

yielding a light-blue transparent colloidal dispersion (see Supporting Information for further details).

The absorption spectra for ZnPc in phosphate buffer (0.2 M, pH 5.7) were recorded in the absence and presence of Brij 98 (Figure 1a). In the absence of Brij 98, the water-insoluble ZnPc exists as a relatively coarse suspension even after sonication: intense light scattering from such macroscopic ZnPc aggregates leads to a broad, featureless absorption spectrum. Conversely, the microscopic ZnPc aggregates obtained in the presence of Brij 98 scatter much less light: a well-defined absorption band is observed in the absorption spectrum at 675 nm along with additional vibronic features. Furthermore, an intense fluorescence ZnPc signal at 678 nm is only obtained in the presence of Brij 98 (Figure 1b). These results indicate that Brij 98 acts as an effective surfactant/dispersant for ZnPc with the resulting relatively small particles potentially enabling enhanced photocatalytic performance. Transmission electron microscopy (TEM) studies (Figure 1c) revealed well-dispersed spherical particles with a mean diameter of 363 ± 47 nm (based on the analysis of 50 particles).

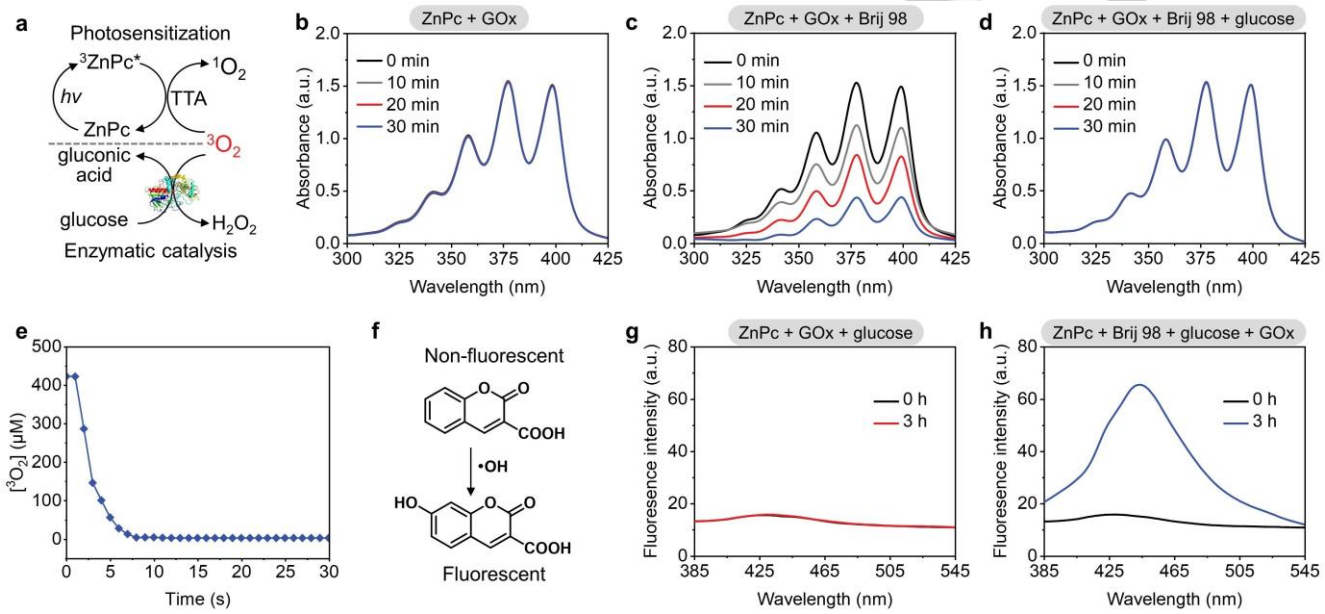

Figure 2. a) Competitive utilization of $^3O_2$ by photosensitization vs. enzymatic catalysis. b−d) Detection of $^1O_2$ using 3,3′-(anthracene-9,10-diyl) dipropanoic acid (ADPA) as a probe: UV-visible absorption spectra recorded for ADPA using various formulations. e) Evolution of $^3O_2$ concentration in the solution. f) Mechanism of hydroxyl radical trapping by CCA for fluoresence detection. g−h) Fluorescence spectra of CCA-hydroxyl radical adduct recorded after irradiation for different times (excitation wavelength = 370 nm). Test conditions: [ADPA] = 0.2 mM, [ZnPc] = 12 μM, [Brij 98] = 0 or 10 mg mL^{-1}, [GOx] = 150 U mL^{-1}, [glucose] = 0 or 20 mM, phosphate buffer (0.2 M, pH 5.7), NIR light (λ_{max} = 730 nm; I = 140 mW cm^{-2}), [CCA] = 1 mM.

To construct the enzyme-NIR cascade, we opted to utilize GOx for oxygen scavenging and H_2O_2 generation owing to its high stability and efficiency.[16] However, the triplet excited state of ZnPc (^{3}ZnPc*) is also capable of undergoing triplet–triplet annihilation (TTA), converting triplet oxygen ($^3O_2$) into singlet oxygen ($^1O_2$). Hence there are two possible pathways for $^3O_2$ consumption for this system: enzymatic catalysis and photosensitization (Figure 2a). To differentiate between these two pathways, 3,3′-(anthracene-9,10-diyl) dipropanoic acid (ADPA) was used as a specific probe for $^1O_2$ detection by UV-visible absorption spectroscopy (Figure S1).[17] When a system containing just ZnPc and GOx (i.e., no Brij 98 surfactant) was irradiated with NIR light (λ_{max} = 730 nm), no change in the ADPA spectrum was observed over a 30 min period (Figure 2b), indicating that no $^1O_2$ was produced. This suggests that the insoluble ZnPc in aqueous solution impairs its ability to photosensitize $^3O_2$. In contrast, the absorption of ADPA at 325−425 nm is significantly reduced when employing Brij 98-stabilized ZnPc particles in the presence of GOx (Figure 2c). This indicates that Brij 98-stabilized ZnPc particles maintained the ability for $^3O_2$ photosensitization. However, addition of glucose to this latter formulation resulted in no detectable $^1O_2$ production (Figure 2d), suggesting that GOx deoxygenation is the predominant $^3O_2$ consumption pathway compared to ZnPc photosensitization. Indeed, using an online detection oxygen sensor to monitor the aqueous solution revealed that $^3O_2$ was almost fully consumed by GOx within approximately 5 seconds (Figure 2e).

This rapid GOx deoxygenation produces H_2O_2, which is subsequently used to generate hydroxyl radicals via ZnPc photosensitization. The latter reaction was monitored by fluorescence spectroscopy using coumarin-3-carboxylic acid (CCA) as a specific probe for hydroxyl radicals (Figure 2f).[18] As expected, the macroscopic ZnPc aggregates did not generate any hydroxyl radicals, as evidenced by Figure 2g. In contrast, the microscopic Brij 98-stabilized ZnPc particles produced strong fluorescence when irradiated with NIR light (Figure 2h). This suggests that Brij 98-stabilized ZnPc particles are effective photosensitizers for the conversion of H_2O_2 into hydroxyl radicals. In principle, such an enzyme-NIR cascade could be potentially employed for RAFT polymerization in aqueous media.

High-throughput RAFT polymerizations using ZnPc particles

After establishing the enzyme-NIR cascade catalysis reactions, we applied this system to aqueous RAFT polymerization (Figures 3 and S2). The remarkable deoxygenation capacity of GOx allows high-throughput RAFT polymerization to be conducted under

benchtop conditions, facilitating reaction optimization with minimal materials consumption.[19] *N*,*N*-Dimethylacrylamide (DMA) and 4-((((2-carboxyethyl)thio)carbonothioyl)thio)-4-cyanopentanoic acid (CTPA) were selected as the representative monomer and RAFT agent owing to their matched reactivities and high solubility in phosphate buffer.

When targeting a degree of polymerization (DP) of 500 using the macroscopic ZnPc aggregates, only 14% DMA conversion was achieved after NIR light irradiation for 12 h (Table S1, #1). In contrast, 58% DMA conversion was obtained under the same conditions when using the microscopic ZnPc particles (Brij 98 = 10 mg mL^{-1}). Because Brij 98 plays a crucial role in producing such microscopic particles, we examined the effect of Brij 98 concentration on the polymerization kinetics (Figure 3a; Tables S3−S6). Pseudo-first order kinetics were observed for the polymerizations conducted in the presence of Brij 98. On doubling this surfactant's concentration from 5 to 10 mg mL^{-1}, the apparent propagation constant (k_p^{app}) increased from 0.077 to 0.085 h^{-1} at 70 mW cm^{-2}. Increasing the light intensity from 70 mW cm^{-2} to 140 mW cm^{-2} led to a further rate enhancement (k_p^{app} = 0.119 h^{-1}). However, using a Brij 98 concentration of 20 mg mL^{-1} did not lead to a faster rate of polymerization at 140 mW cm^{-2} (k_p^{app} = 0.120 h^{-1}), despite higher Brij 98 concentrations leading to stronger light absorption by ZnPc particles (Figure S14). In this case, H_2O_2 production by slow oxygen diffusion from the headspace became the rate-limiting step when sufficiently high Brij 98 concentration was used to improve the ZnPc light absorption efficiency.

Remarkably, GPC analysis confirmed that the molecular weights were close to the theoretical values while dispersities were relatively low in all cases ($Đ$ < 1.2), see Figures S7, S9, S11 and S13. It is also worth emphasizing that RAFT control was not adversely affected by the presence of Brij 98. Importantly, control experiments conducted in the absence of any ZnPc confirmed that neither NIR illumination nor Brij 98 were able to initiate background polymerization (Figure 3a, gray line; Table S7, Figure S15).

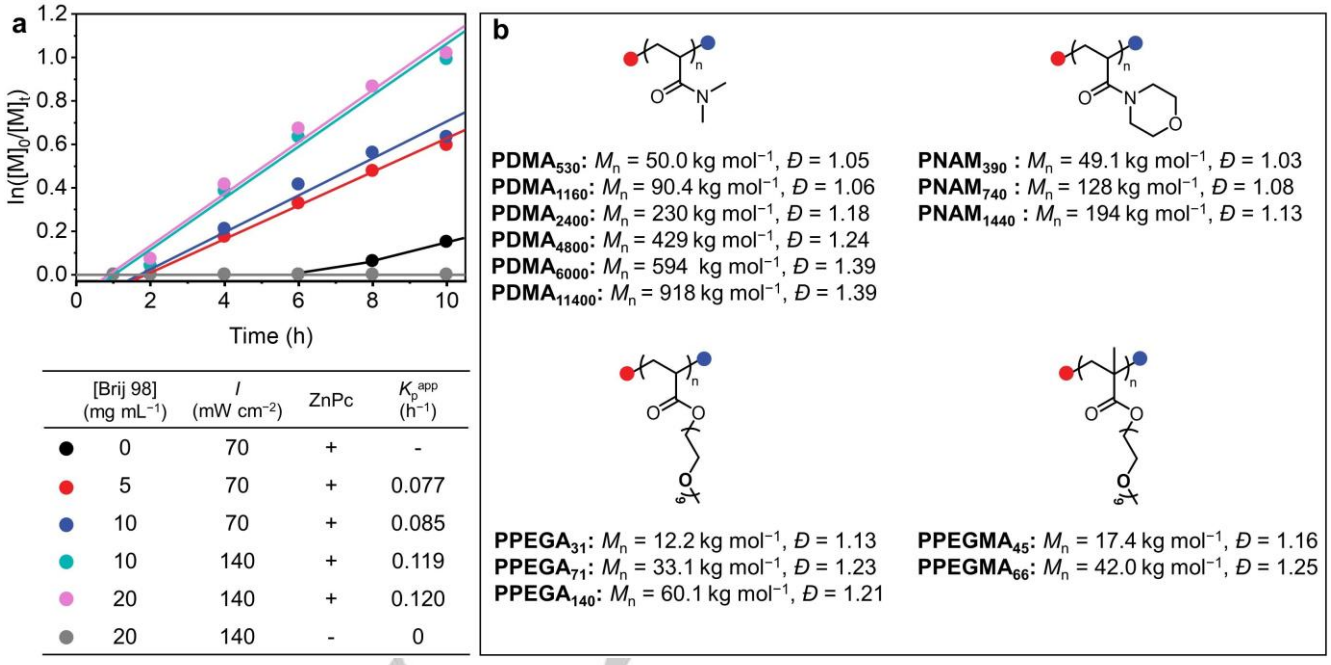

Figure 3. High-throughput RAFT polymerization conducted in a 96-well plate using enzyme-NIR cascade catalysis. a) Polymerization kinetics data for DMA obtained under various conditions. b) Summary of molecular weights and dispersities for the various target polymers. Polymerization conditions: 300 µL, [monomer] = 30% w/v, [GOx] = 150 U mL^{-1}, [glucose] = 20 mM, [ZnPc] = 0 or 4 ppm, [Brij 98] = 5−20 mg mL^{-1}, NIR light (λ_{max} = 730 nm).

To illustrate the capacity of the enzyme-NIR system for the high-throughput synthesis of well-defined polymers, a library of polymers based on four different vinyl monomers was prepared in 96-well plates (Figure 3b) with moderate (53%) to high (89%) conversions (Table S8) when targeting various molecular weights. For example, DMA polymerizations performed when targeting DPs of 1,000−20,000 yielded low-dispersity polymers with molecular weights ranging from 50.0 to 918 kg mol^{-1}. Moreover, such homopolymers could be obtained at remarkably low photocatalyst loadings (4 ppm). A kinetic study conducted for a DMA polymerization when targeting a DP of 15,000 revealed a pseudo-first-order kinetic plot and a well-controlled RAFT process, as evidenced by low dispersities and the close match between experimental and theoretical molecular weights (Table S9, Figures S17−S18). *N*-Acryloylmorpholine (NAM), poly(ethylene glycol) methyl ether acrylate (PEGA, M_n = 480 g mol^{-1}), and poly(ethylene glycol) methyl ether methacrylate (PEGMA, M_n = 500 g mol^{-1}) were also evaluated under the similar conditions, yielding low-dispersity homopolymers ($Đ$ ≤ 1.25) along with predictable molecular weights (Figure S16).

Next, we extended this new method to block copolymer syntheses in order to examine chain-end fidelity. Two pseudo-block copolymers ($PDMA_{350}$-*b*-$PDMA_{250}$ and $PNAM_{300}$-*b*-$PNAM_{325}$) were prepared by sequential addition of monomer. In both cases, GPC analysis confirmed a significant increase in molecular weight with no tailing (Figure S19), which indicates excellent chain-end fidelity.

Temporal control over this polymerization system was also demonstrated by switching the NIR light on/off (Figure 4a, Table S10). After conducting a NIR-mediated DMA polymerization for 3 h, the light source was turned off for a 2 h interval. NMR spectroscopic analysis indicated that the monomer conversion

(15%) remained unchanged in the absence of any NIR irradiation. Upon resuming irradiation for 1 h, the monomer conversion increased from 15% to 34%. Repeating the aforementioned "on/off" protocol confirmed that polymerization only occurred during NIR irradiation, and the polymerization remained temporarily dormant in the absence of this light source. The corresponding GPC analysis (Figure 4b) showed that the molecular weight remained unchanged during the light-off period, while exposure to light resulted in an increase in molecular weight. Moreover, multiple light switching did not reduce the controllable character of this DMA polymerization.

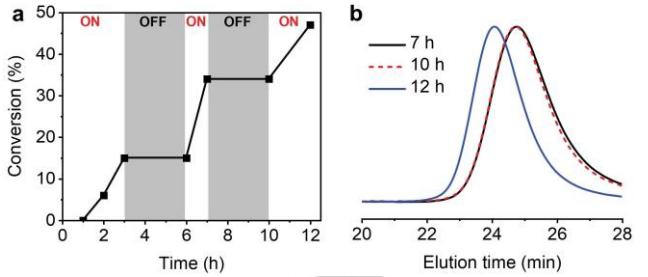

Figure 4. Results of "on/off" polymerization. a) Plot of DMA conversion *versus* time. b) GPC traces recorded for polymers obtained at different reaction times. Polymerization conditions: 300 µL, [DMA] = 30% w/v, [CTPA]/[DMA] = 1:500, [GOx] = 150 U mL^{-1}, [glucose] = 20 mM, [ZnPc] = 4 ppm, [Brij 98] = 10 mg mL^{-1}, NIR light (λ_{max} = 730 nm, *I* = 140 mW cm^{-2}).

RAFT polymerizations using ZnTtBNc particles

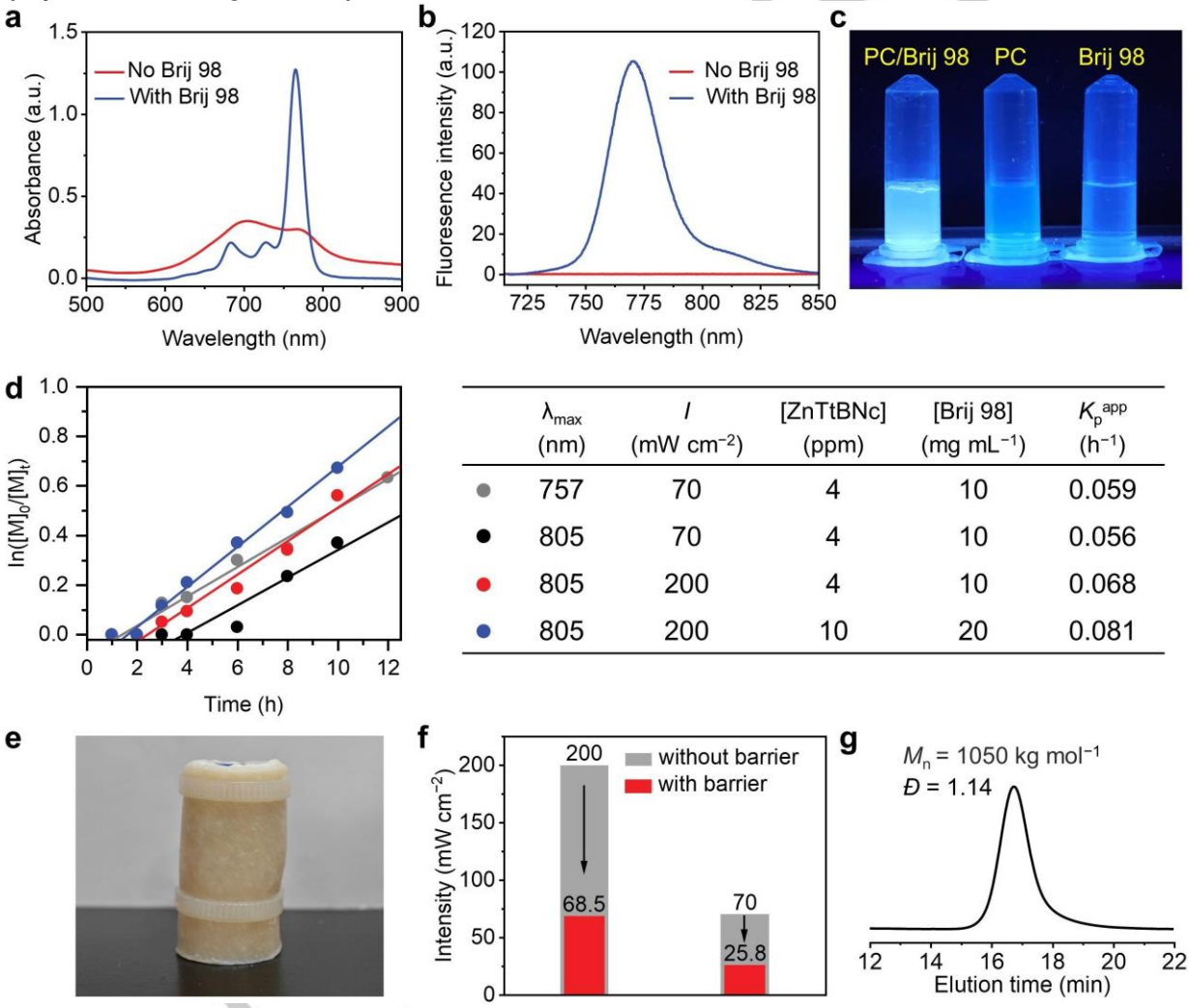

	λ_{max} (nm)	*I* (mW cm^{-2})	[ZnTtBNc] (ppm)	[Brij 98] (mg mL^{-1})	K_p^{app} (h^{-1})
●	757	70	4	10	0.059
●	805	70	4	10	0.056
●	805	200	4	10	0.068
●	805	200	10	20	0.081

Figure 5. a) Visible absorption and b) fluorescence spectra (excitation wavelength = 700 nm) recorded for ZnTtBNc in the absence or presence of Brij 98 in phosphate buffer (0.2 M, pH 5.7). c) Digital photographs of phosphate buffer containing three different formulations on excitation with 365 nm light. PC = ZnTtBNc. [ZnTtBNc] = 0 or 12 µM, [Brij 98] = 0 or 10 mg mL^{-1}. d) Polymerization kinetics data obtained under different conditions using ZnTtBNc particles. e) Digital photograph of a 2 mL reaction vial covered with 5 mm-thick porcine skin. f). Intensity reduction of the 805 nm NIR light after penetrating 5 mm-thick porcine skin. g) GPC trace of UHMW PDMA prepared using ZnTtBNc particles at 25.8 mW cm^{-2}.

To broaden the applicability of surfactant-stabilized hydrophobic NIR photocatalysts, we selected zinc 2,11,20,29-*tetra*-*tert*-butyl-2,3-naphthalocyanine (ZnTtBNc) as an alternative candidate. Compared to ZnPc, ZnTtBNc exhibits a significantly red-shifted absorption, which should lead to enhanced NIR absorption. However, ZnTtBNc's more extensive conjugation leads to greater hydrophobic character, which severely limits its aqueous solubility. Fortunately, our new colloidal stabilization strategy proved equally effective for ZnTtBNc (Figures 5a and 5b). Thus, a Brij 98-ZnTtBNc colloidal dispersion exhibited enhanced

fluorescence compared to its corresponding coarse suspension (Figure 5c) owing to the much smaller particle size (433 ± 58 nm) in the former case (Figure S20).

ZnTtBNc was subsequently used as a photocatalyst for RAFT polymerization of DMA under NIR light irradiation (λ_{max} = 757 nm or 805 nm). Control experiments confirmed that using ZnTtBNc alone resulted in no polymerization (Table S11, #1), but the Brij 98-stabilized ZnTtBNc particles resulted in 17% DMA conversion, presumably by a photoinduced electron/energy transfer (PET) mechanism (Table S11, #2).[20] When the complete enzyme-NIR formulation (i.e., GOx, glucose, Brij 98-stabilized ZnTtBNc particles) was used, a DMA conversion of 50% was achieved (Table S11, #4), which demonstrates the potential of Brij 98-stabilized ZnTtBNc particles as a viable photocatalyst for NIR photocontrolled RAFT polymerization.

Compared to ZnPc, ZnTtBNc's red-shifted absorption spectrum allows the use of NIR light sources with longer wavelengths (λ_{max} = 757 nm or 805 nm) for polymerization kinetic studies (Tables S12−S15, Figures S21−S28). Under otherwise identical conditions, the polymerization achieved using NIR irradiation at 805 nm was slower than that obtained using 757 nm light (Figure 5d). Moreover, the former synthesis exhibited a longer induction period (4 h *vs.* 1 h), presumably owing to its lower photon energy as well as the reduction in overlap with the ZnTtBNc absorption band. Increasing the light intensity and ZnTtBNc and Brij 98 concentrations led to shorter induction periods and faster polymerizations. After a certain (variable) induction period, all polymerizations exhibited pseudo-first order kinetics, predictable molecular weights and low dispersities (Figures S22, S24, S26, and S28).

To demonstrate the biological penetration capability, we performed RAFT polymerization through a 5-mm porcine skin barrier using NIR light at 805 nm (Figure 5e). To explore the synthetic limits of this enzyme-NIR system, we targeted the synthesis of UHMW PDMA homopolymers ([CTPA]/[DMA] = 1:20,000) at light intensities of either 200 mW cm^{-2} or 70 mW cm^{-2}. In the latter case, the initial light intensity was reduced to 25.8 mW cm^{-2} after penetrating the porcine skin barrier (Figure 5f), producing an UHMW polymer (1,020 kg mol^{-1}; $Đ$ = 1.19) (Table S16, Figure S29). Interestingly, a lower molecular weight polymer (737 kg mol^{-1}; $Đ$ = 1.19) was obtained when employing the 200 mW cm^{-2} light source, despite its significantly higher intensity (68.5 mW cm^{-2}) after passing through the porcine skin barrier. Notably, control experiments performed without any skin barrier did not produce UHMW polymers when using either the 200 mW cm^{-2} or 70 mW cm^{-2} light source. This suggests that there is an optimal light intensity (e.g., 25.8 mW cm^{-2}) that favors the formation of UHMW polymers owing to the controlled and sustained rate of production of radicals.[19b, 21] Indeed, a DMA polymerization conducted by direct irradiation at 25.8 mW cm^{-2} also produced a low-dispersity UHMW homopolymer (Figure 5g, Table S17). The ability to synthesize UHMW polymers through biological barriers opens up new avenues for biologically relevant applications.

Conclusion

We demonstrate that hydrophobic NIR photocatalysts can be dispersed as colloidally stable particles in water, thereby enabling their catalytic function to be harnessed for aqueous RAFT polymerization. An enzyme-NIR cascade catalysis system consisting of GOx deoxygenation and NIR photosensitization was developed for high-throughput RAFT polymerization, yielding well-defined polymers from various vinyl monomers across a broad range of molecular weights. This enzyme-NIR system offers multiple benefits, including oxygen tolerance, environmental friendliness, and low catalyst loadings. The ability to generate low-dispersity UHMW polymers through biological barriers suggests that this new approach offers considerable potential for biomaterials engieering. Considering the diversity of available surfactants and hydrophobic catalysts, our strategy can be extended to include a wide range of photocatalyst platforms, enabling tailored light wavelengths to be used in photocontrolled polymer synthesis in biologically relevant media.

Acknowledgements

We thank for the financial support by the National Key R&D Program of China (2021YFA1501600) and the National Natural Science Foundation of China (22193020, 22193024, 22371089). Ruoyu Li acknowledges a two-year financial support by the Postdoctoral Fellowship Program of CPSF under GZB20250247.

Keywords: NIR • enzyme catalysis • radical polymerization • RAFT • high-throughput polymerization

[1] a) K. Parkatzidis, H. S. Wang, N. P. Truong, A. Anastasaki, *Chem* **2020**, *6*, 1575-1588; b) N. P. Truong, G. R. Jones, K. G. E. Bradford, D. Konkolewicz, A. Anastasaki, *Nature Reviews Chemistry* **2021**, *5*, 859-869; c) J. Chiefari, Y. K. Chong, F. Ercole, J. Krstina, J. Jeffery, T. P. T. Le, R. T. A. Mayadunne, G. F. Meijs, C. L. Moad, G. Moad, E. Rizzardo, S. H. Thang, *Macromolecules* **1998**, *31*, 5559-5562; d) *Macromolecules* **2017**, *50*, 9525-9527; e) N. G. Engelis, A. Anastasaki, G. Nurumbetov, N. P. Truong, V. Nikolaou, A. Shegiwal, M. R. Whittaker, T. P. Davis, D. M. Haddleton, *Nature Chemistry* **2017**, *9*, 171-178; f) X.-l. Qin, Z.-s. An, *Acta Polymerica Sinica* **2024**, *55*, 67-78; g) Y. Zhao, S. Zhang, Z. An, *Angewandte Chemie International Edition* **2025**, *64*, e202421851.

[2] a) Y. Lee, C. Boyer, M. S. Kwon, *Chemical Society Reviews* **2023**, *52*, 3035-3097; b) Q. Wang, F.-Y. Bai, Y. Wang, F. Niu, Y. Zhang, Q. Mi, K. Hu, X. Pan, *Journal of the American Chemical Society* **2022**, *144*, 19942-19952; c) J. C. Theriot, C.-H. Lim, H. Yang, M. D. Ryan, C. B. Musgrave, G. M. Miyake, *Science* **2016**, *352*, 1082-1086; d) Q. Ma, J. Song, X. Zhang, Y. Jiang, L. Ji, S. Liao, *Nature Communications* **2021**, *12*, 429; e) M. E. Lott, L. Trachsel, E. Schué, C. L. G. I. V. Davidson, R. A. Olson S, D. I. Pedro, F. Chang, Y. Hong, W. G. Sawyer, B. S. Sumerlin, *Macromolecules* **2024**, *57*, 4007-4015; f) C. Aydogan, G. Yilmaz, A. Shegiwal, D. M. Haddleton, Y. Yagci, *Angewandte Chemie International Edition* **2022**, *61*, e202117377; g) Q. Ma, G. G. Qiao, Z. An, *Angewandte Chemie International Edition* **2023**, *62*, e202314729; h) M. Chen, M. Zhong, J. A. Johnson, *Chemical Reviews* **2016**, *116*, 10167-10211; i) S. Lian, S. P. Armes, Z. An, *CCS Chemistry* **2025**, doi.org/10.31635/ccschem.31024.202404894; j) S.-t. Han, M.-l. Xu, M. Chen, *Acta Polymerica Sinica* **2024**, *55*, 841-855.

[3] a) H. Wang, Q. Li, J. Dai, F. Du, H. Zheng, R. Bai, *Macromolecules* **2013**, *46*, 2576-2582; b) L. Lu, H. Zhang, N. Yang, Y. Cai, *Macromolecules* **2006**, *39*, 3770-3776; c) E. Yousif, R. Haddad, *SpringerPlus* **2013**, *2*, 398; d) M. Zhang, S. P. Armes, Z. An, *Macromolecules* **2025**, *58*, 507-515; e) Z. Qing, W. Wang, R. Li, Z. An, *Macromolecules* **2025**, *58*, 6771-6780.

[4] a) S. Shanmugam, J. Xu, C. Boyer, *Angewandte Chemie International Edition* **2016**, *55*, 1036-1040; b) B. D. Ravetz, A. B. Pun, E. M. Churchill, D. N. Congreve, T. Rovis, L. M. Campos, *Nature* **2019**, *565*, 343-346.

[5] a) Y. Chen, J. Zhang, X. Liu, S. Wang, J. Tao, Y. Huang, W. Wu, Y. Li, K. Zhou, X. Wei, S. Chen, X. Li, X. Xu, L. Cardon, Z. Qian, M.

Gou, *Science Advances* **2020**, *6*, eaba7406; b) B. Ran, Z. Wang, W. Cai, L. Ran, W. Xia, W. Liu, X. Peng, *Journal of the American Chemical Society* **2021**, *143*, 17891-17909; c) Y. Wan, L.-H. Fu, C. Li, J. Lin, P. Huang, *Advanced Materials* **2021**, *33*, 2103978; d) K.-X. Teng, W.-K. Chen, L.-Y. Niu, W.-H. Fang, G. Cui, Q.-Z. Yang, *Angewandte Chemie International Edition* **2021**, *60*, 19912-19920.

[6] a) Q. Ti, L. Fang, W. Zhao, L. Bai, H. Zhao, X. Ba, W. Chen, *Journal of the American Chemical Society* **2023**, *145*, 26160-26168; b) H. Cao, G. Wang, Y. Xue, G. Yang, J. Tian, F. Liu, W. Zhang, *ACS Macro Letters* **2019**, *8*, 616-622; c) J. Jiang, G. Ye, F. Lorandi, Z. Liu, Y. Liu, T. Hu, J. Chen, Y. Lu, K. Matyjaszewski, *Angewandte Chemie International Edition* **2019**, *58*, 12096-12101; d) Y. Deng, C. Li, J. Fan, X. Guo, *Macromolecular Rapid Communications* **2023**, *44*, 2300258; e) H. Zha, L. Cheng, Z. Wang, C. Liu, C. Hong, *Science China Chemistry* **2024**, *67*, 2353-2361; f) Z. Wu, C. Boyer, *Advanced Science* **2023**, *10*, 2304942; g) Z. Wu, T. Zhang, X. Shi, N. Corrigan, G. Ng, C. Boyer, *Angewandte Chemie International Edition* **2023**, *62*, e202302451.

[7] S. Allison-Logan, Q. Fu, Y. Sun, M. Liu, J. Xie, J. Tang, G. G. Qiao, *Angewandte Chemie International Edition* **2020**, *59*, 21392-21396.

[8] a) Z. Wu, W. Fang, C. Wu, N. Corrigan, T. Zhang, S. Xu, C. Boyer, *Chemical Science* **2022**, *13*, 11519-11532; b) G. Ng, Z. Wu, T. Zhang, A. P. Dang, Y. Yao, A. R. J. Nelson, S. W. Prescott, A. Postma, G. Moad, C. J. Hawker, C. Boyer, *Macromolecules* **2023**, *56*, 7898-7908.

[9] J. Sun, S. Ren, H. Zhao, S. Zhang, X. Xu, L. Zhang, Z. Cheng, *ACS Macro Letters* **2023**, *12*, 165-171.

[10] X. Hu, G. Szczepaniak, A. Lewandowska-Andralojc, J. Jeong, B. Li, H. Murata, R. Yin, A. M. Jazani, S. R. Das, K. Matyjaszewski, *Journal of the American Chemical Society* **2023**, *145*, 24315-24327.

[11] a) S. Lian, R. Li, Y. Chen, Z. An, *Macromolecules* **2025**, *58*, 5385-5394; b) S. Zhu, W. Kong, S. Lian, A. Shen, S. P. Armes, Z. An, *Nature Synthesis* **2025**, *4*, 15-30; c) H. Gong, Y. Gu, Y. Zhao, Q. Quan, S. Han, M. Chen, *Angewandte Chemie International Edition* **2020**, *59*, 919-927; d) C. B. Eades, K. C. Stevens, D. E. Cabrera, M. K. Vereb, M. E. Lott, J. I. Bowman, B. S. Sumerlin, *Chemical Science* **2025**, *16*, 5573-5578.

[12] a) C. Kütahya, C. Schmitz, V. Strehmel, Y. Yagci, B. Strehmel, *Angewandte Chemie International Edition* **2018**, *57*, 7898-7902; b) W. F. Wei, W. L. Guo, M. Jian, L. S. Qin, X. Li, T. Cai, *Chemical Engineering Journal* **2023**, *455*, 140631.

[13] a) J. Wang, Z. Wang, Y. Zhong, Y. Zou, C. Wang, H. Wu, A. Lee, W. Yang, X. Wang, Y. Liu, D. Zhang, J. Yan, M. Hao, M. Zheng, R. Chung, F. Bai, B. Shi, *Biomaterials* **2020**, *229*, 119576; b) J. F. Lovell, C. S. Jin, E. Huynh, H. Jin, C. Kim, J. L. Rubinstein, W. C. W. Chan, W. Cao, L. V. Wang, G. Zheng, *Nature Materials* **2011**, *10*, 324-332; c) X. Li, X.-H. Peng, B.-D. Zheng, J. Tang, Y. Zhao, B.-Y. Zheng, M.-R. Ke, J.-D. Huang, *Chemical Science* **2018**, *9*, 2098-2104.

[14] a) T. G. Gantchev, I. J. Urumov, D. J. Hunting, J. E. Van Lier, *International Journal of Radiation Biology* **1994**, *65*, 289-298; b) T. G. Gantchev, J. E. van Lier, *Chemical Physics Letters* **2003**, *369*, 627-634.

[15] S. Bhattacharya, S. DasChowdhury, *Colloid and Polymer Science* **2024**, *302*, 1603-1616.

[16] a) B. Zhang, X. Wang, A. Zhu, K. Ma, Y. Lv, X. Wang, Z. An, *Macromolecules* **2015**, *48*, 7792-7802; b) R. Li, W. Kong, Z. An, *Angewandte Chemie International Edition* **2022**, *61*, e202202033; c) W. Kong, Z. An, *CCS Chemistry* **2025**, doi:10.31635/ccschem.31025.202505832.

[17] B. Yuan, H. Wang, J.-F. Xu, X. Zhang, *ACS Applied Materials & Interfaces* **2020**, *12*, 26982-26990.

[18] B. Tang, J. Zhao, Y. Jiao, J.-F. Xu, X. Zhang, *Chemical Communications* **2019**, *55*, 14127-14130.

[19] a) R. Chapman, A. J. Gormley, M. H. Stenzel, M. M. Stevens, *Angewandte Chemie International Edition* **2016**, *55*, 4500-4503; b) R. Li, S. Zhang, Q. Li, G. G. Qiao, Z. An, *Angewandte Chemie International Edition* **2022**, *61*, e202213396.

[20] Z. Wu, K. Jung, C. Wu, G. Ng, L. Wang, J. Liu, C. Boyer, *Journal of the American Chemical Society* **2022**, *144*, 995-1005.

[21] A. Reyhani, S. Allison-Logan, H. Ranji-Burachaloo, T. G. McKenzie, G. Bryant, G. G. Qiao, *Journal of Polymer Science Part A: Polymer Chemistry* **2019**, *57*, 1922-1930.

Entry for the Table of Contents

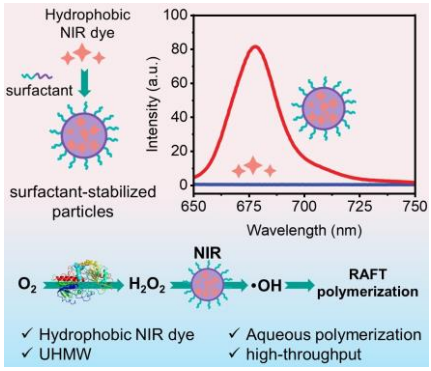

Colloidal particles prepared from hydrophobic NIR photocatalysts exhibit catalytic function in aqueous solution. The enzymatic catalysis and colloidal particles constitute a new enzyme-NIR cascade catalysis system for efficient high-throughput RAFT polymerization.